Nanoscale Res Lett (2006) 1:120–136
DOI 10.1007/s11671-006-9000-1

NANO REVIEW

Unbound states in quantum heterostructures

R. Ferreira · G. Bastard

Published online: 27 September 2006

Abstract We report in this review on the electronic continuum states of semiconductor Quantum Wells and Quantum Dots and highlight the decisive part played by the virtual bound states in the optical properties of these structures. The two particles continuum states of Quantum Dots control the decoherence of the excited electron – hole states. The part played by Auger scattering in Quantum Dots is also discussed.

Keywords Virtual bound states · Quantum Dots · Quantum Wells · Decoherence · Auger effect · Photodetectors

Introduction

A number of modern opto-electronics devices involve low dimensional semiconductor heterostructures. In Quantum well (QW) lasers, for instance, the electron–hole recombination involves electrons and holes that are bound along the growth axis of the heterostructure but free to move in the layer planes. In a quantum dot (QD) laser the recombination takes place between electrons and holes that are bound along the three directions of space [1]. Yet, whatever the dimensionality of the carrier motion in the lasing medium, the feeding of the QW or QD lasers with carriers by electrical injection occurs from the bulk-like contacts through heterostructure electron/hole states that are spatially extended. Along the same line, in an unipolar QD-based photo-detector, the initial state is bound, the final state is delocalized. It is not often realized that the continuum of these extended states may show structure and that the eigenstates corresponding to certain energy regions of the continuum may display abnormally large amplitudes where the bound states are mainly localized in the heterostructures, thereby being prevalent in the phenomena of capture processes.

When looking at zero-dimensional heterostructures (QDs), it may also well happen that there exist bound two-particle states (e.g., electron–hole or two electron states) that are superimposed to a two particle continuum. This feature is as a rule a necessity and recalls, e.g., the ionization states of two electron atoms like He. In the context of QDs, the occurrence of bound electron–hole states interacting with a continuum gives rise to a number of important features, like increased decoherence and line broadening, changes in shape of the absorption coefficient. All these signatures have been experimentally evidenced.

In this short review, we shall present some of the recent findings about the continuum states of semiconductor heterostructures. In Sect. 2, we recall the QW continuum states. Then, in Sect. 3 we switch to the continuum states of the QD single particle spectrum, in particular the part they play in the phonon-assisted capture and in the photo-detection of far infrared light. Section 4 will be devoted to the two particle continuum states of QDs and to their role in ejecting carriers that were already bound to the QD.

R. Ferreira (✉) · G. Bastard
Laboratoire Pierre Aigrain, Ecole Normale Supérieure,
24 rue Lhomond, F-75005 Paris, France
e-mail: wei.wu@boku.ac.at

G. Bastard
Institute of Industrial Sciences, Tokyo University, 4-6-1
Komaba, Meguro-kuTokyo 153-8505, Japan
e-mail: gerald.bastard@lpa.ens.fr

The continuum states of quantum wells

Throughout this review, we shall confine ourselves to an envelope description of the one electron states. Further, we shall for simplicity use a one band effective mass description of the carrier kinematics in the heterostructures. Multi-band description [2] can be very accurate for the bound states, in fact as accurate as the atomistic-like approaches [3–5]. To our knowledge, the continuum states have not received enough attention to allow a clear comparison between the various sorts of theoretical approaches. Their nature is intricate enough to try in a first attempt a simplified description of their properties.

In a square quantum well, the Hamiltonian is:

$$H = \frac{p_z^2}{2m^*} + \frac{p_x^2}{2m^*} + \frac{p_y^2}{2m^*} + V_{\mathrm{b}}(z), \tag{1}$$

where m^* is the carrier effective mass, taken as isotropic and position independent for simplicity. The potential energy $V_{\mathrm{b}}(z)$ is $-V_{\mathrm{b}}$ in the well and 0 in the barrier ($|z| > w/2$, where w is the well width). Because of the translational invariance in the layer plane, the total eigenstates are of the form

$$\Psi(x,y,z) = \frac{e^{i(k_x x + k_y y)}}{\sqrt{S}}\chi(z)$$

$$\varepsilon = \frac{\hbar^2}{2m^*}(k_x^2 + k_y^2) + \varepsilon_z \tag{2}$$

where $\boldsymbol{k} = (k_x, k_y)$ is the wave-vector related to the free in-plane motion, S the layer (normalization) surface and ε_z and $\chi(z)$ are solutions of the one-dimensional (1D) Hamiltonian :

$$\left[\frac{p_z^2}{2m^*} + V_{\mathrm{b}}(z)\right]\chi(z) = \varepsilon_z\chi(z) \tag{3}$$

Hence, disregarding the in-plane motion, one finds bound states (energies $\varepsilon_z < 0$) that are non-degenerate and necessarily odd or even in z (see e.g., [5–8]). For energies $\varepsilon_z > 0$ the states are unbound. They are twice degenerate and correspond classically to an electron impinging on the well, being suddenly accelerated at the interface then moving at fixed velocity in the well, being suddenly decelerated at the second interface and moving away from the well at constant speed. Classically, the time delay experienced by the electron because of the well is therefore negative. Quantum mechanically, one can exploit the analogy between the time independent Schrödinger equation and the propagation of electromagnetic fields that are harmonic in time (see e.g., [9]). Then, the continuous electronic spectrum of the square well problem translates into finding the solutions of Maxwell equations in a Perot–Fabry structure (see e.g., [10]). We shall therefore write the solution for $\varepsilon_z > 0$ in the form:

$$\begin{array}{ll} \chi_+(z) = e^{ik_b(z+w/2)} + re^{ik_b(z+w/2)} & z \le -w/2 \\ \chi_+(z) = \alpha e^{ik_w z} + \beta e^{-ik_w z} & |z| \le w/2 \\ \chi_+(z) = te^{ik_b(z-w/2)} & z \ge w/2 \end{array} \tag{4}$$

for a propagation from the left to the right. Here, k_{b} and k_{w} are the electron wavevectors in the barrier and in the well, respectively:

$$k_{\mathrm{w}} = \sqrt{\frac{2m^*(\varepsilon_z + V_{\mathrm{b}})}{\hbar^2}}; \quad k_b = \sqrt{\frac{2m^*\varepsilon_z}{\hbar^2}} \tag{5}$$

The coefficients r and t are the amplitude reflection and transmission coefficients, respectively. The intensity coefficients are, respectively, R and T with:

$$R = |r|^2; \quad T = |t|^2; \quad R + T = 1 \tag{6}$$

There exists a $\chi_-(z)$ solution at the same energy ε_z as $\chi_+(z)$. It corresponds to an electron motion from the right to the left. Neither χ_+, nor χ_- is an eigenfunction of the parity operator with respect to the center of the well. Sometimes, it is desirable to get those solutions (e.g., in order to evaluate the bound-to-continuum optical absorption in the electric dipole approximation). One then takes the normalized symmetrical (even states) or anti-symmetrical (odd states) combinations of χ_+ and χ_- [11].

The χ_+ and χ_- states are not normalizable. One should thus use wavepackets to get properly normalized wavefunctions. These wavepackets can be made reasonably narrow to assimilate them in the barrier or in the well to an almost classical particle moving at a constant velocity. The time evolution of these wavepackets (see Bohm [8] for a throughout discussion) reveals that for most of the energies of the impinging electron, the time delay experienced by the packet due to its crossing of the well is negative, exactly like in the classical description. However, for certain energies there is a considerable slowing down of the packet by the quantum well. In fact, the packet is found to oscillate back and forth in the well, as if it were bound, before finally leaving it. The states for these particular energies are called virtual bound states. They also correspond to the Perot–Fabry transmission resonances:

$$k_{\mathrm{w}} w = p\pi \tag{7}$$

For these particular energies the electron piles up in the well, while it is usually repelled by it, on account that its wavefunction should be orthogonal to all the other solutions, in particular the bound states.

The spatial localization of these particular solutions can also be evidenced by the display of the quantum well projected density of states versus energy [12]. To do so, one first completely discretizes the states for the z motion by closing the structure at $z = \pm L/2$, where $L \gg w$. One then sums over all the available states that have the energy ε, including the in-plane free motion. Since the free motion is bi-dimensional (2D), one should get staircases starting at the energies $\varepsilon = \varepsilon_z$ of the 1D problem. Each of the staircases is weighted by the integrated probability to finding the carrier in the well. The result of such a calculation is shown in Fig. 1. for $L = 300$ nm and several w for electrons ($V_b = 195$ meV; $m^* = 0.067m_0$). For a particle occupying uniformly the available space, the magnitude of each step would be w/L. One sees very clearly that this is not the case for the lower laying continuum energies. In particular, there exist particular energies where the integrated probability in the well is considerably larger than the classical evaluation.

These particular continuum states are thus candidates to play an important role in the phenomenon of capture processes. In such a capture event, a carrier, initially delocalized over the whole structure, undergoes a scattering where its final state is bound to the well. This scattering can be globally elastic (impurity scattering for instance) and thus amounts to transforming kinetic energy for the z motion into in-plane kinetic energy. The scattering can also be inelastic like for instance the absorption or emission of phonons. These phonons are either optical or acoustical. It has been known since a long time that the most efficient inelastic scattering in compounds semiconductors is the emission of longitudinal optical (LO) phonons by the Fröhlich mechanism (see e.g., [13–15]). Since III–V or II–VI semiconductors are partly polar and have most often two different atoms per unit cell, the longitudinal vibrations in phase opposition of these two oppositely charged atoms produce a macroscopic dipolar field. A moving electron responds to this electric field. The interaction Hamiltonian between the electron and the LO phonons reads:

$$H_{\mathrm{e-ph}} = -ie\sqrt{\frac{\hbar\omega_{\mathrm{LO}}}{2\varepsilon_0\Omega}\left(\frac{1}{\varepsilon_\infty}-\frac{1}{\varepsilon_r}\right)}\sum_{\vec{q}}\frac{1}{q}\left(e^{-i\vec{q}.\vec{r}}a_{\vec{q}}^{+}-e^{i\vec{q}.\vec{r}}a_{\vec{q}}\right) \tag{8}$$

where Ω is the sample volume, ε_∞ and ε_r are the high frequency and static dielectric constants, respectively, and the LO phonons have been taken bulk-like and dispersionless. By using the Fermi Golden Rule, we can compute the capture rate of a QW continuum electron due to the emission of a LO phonon versus the

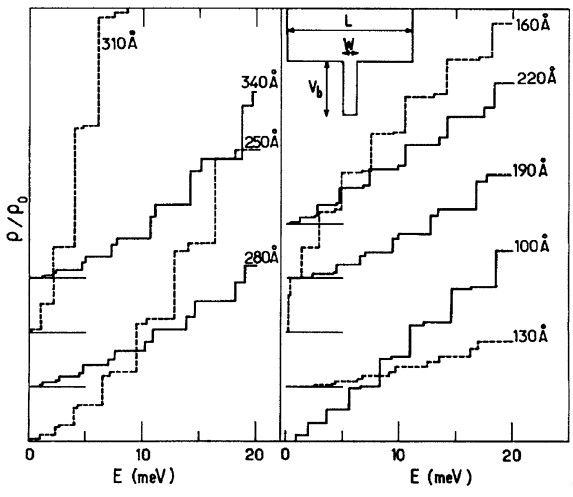

Fig. 1 Quantum-well projected density of states (in units of $\rho_0 = \frac{m*S}{\pi\hbar^2}$) versus energy E. Curves corresponding to different w are displaced vertically for clarity. ρ/ρ_0 varies by 5% between two horizontal divisions. From [12]

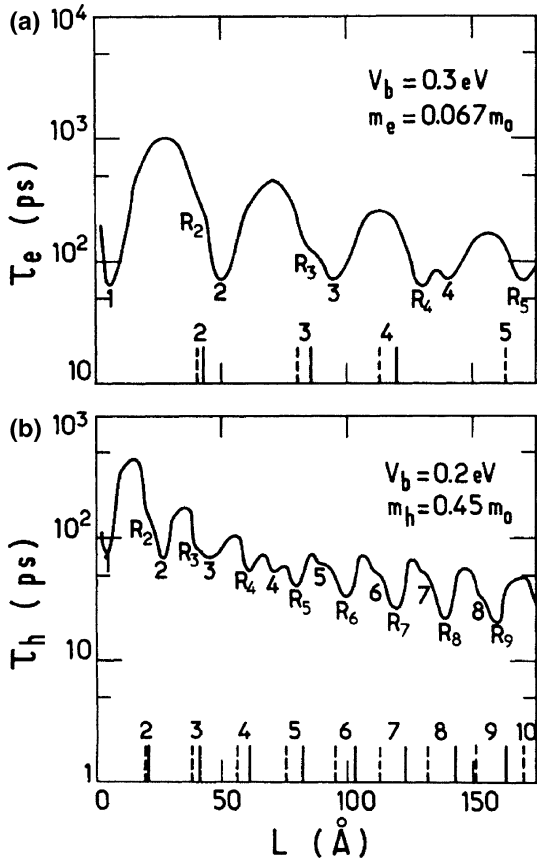

Fig. 2 The average capture times for electrons and holes are plotted versus the QW thickness L for electrons (**a**) and holes (**b**). From [11]

well width w. This rate is averaged over the distribution function of the continuum electron. Figure 2 shows the result of such a computation by assuming that the distribution function is a constant from the edge of the continuum to that edge plus $\hbar\omega_{LO}$ and taking bulk-like phonons [11]. One sees oscillations in the capture time whose amplitude diminishes at large w. Oscillatory capture times were also calculated by Babiker and Ridley [16] in the case of superlattices. These authors also took into account the effect of the superlattice on the optical phonons. Experimentally, to observe the oscillations, one uses time resolved interband photoluminescence: carriers are photocreated in the continuum in a structure that has been lightly doped in order to make sure that the luminescence signal arising from the ground QW transition has a rise time that is dominated by the arrival of the minority carriers. The predicted oscillations were not observed in regular QWs or superlattices because the capture time of electrons and holes was always too short compared to the experimental resolution. Morris et al. [17] however managed to increase it by inserting narrow but high AlAs potential barriers between the GaAs wells and the Ga(Al)As barriers. The slowing down of the capture allowed for a reliable measurement of the capture time. A satisfactory description of the experimental findings (capture time versus well width) was achieved by taking into account the carriers capture by the well due to the emission of LO phonons (see Fig. 3). In actual QW lasers there are many carriers in the barriers or in the wells. They screen the Fröhlich interaction. The screening affects the capture rate and makes it to depend on the carrier concentration. This effect was studied by Sotirelis and Hess [18].

Note finally that the existence of resonant states is not restricted to square well problems. Generally speaking, however, the more sharply varying potentials display the more pronounced resonances.

One electron effects of continuum states in QDs: capture and photo-detection

A vast amount of literature is available in QDs, in particular those grown by Stransky–Krastanov mode (see e.g., [1]). Under such a growth technique a material A (say InAs) is deposited on a substrate B (say GaAs). The lattice constants of the two materials being different (in our specific example 7%), the subsequent growth of A on B accumulates strain energy because the lattice constant of A has to adjust to that of B. There exists a critical thickness of A material beyond which the growth cannot remain bi-dimensional. A 3D growth mode results. Under favorable circumstances this growth gives rise to droplets of A material, called dots or boxes, whose structural parameters (height, radius) depend on the growth conditions (impinging fluxes, substrate temperature, etc....)

The InAs/GaAs dots have received a considerable attention because of their possible applications in telecommunications (lasers, photo-detectors). Even for these well studied objects, there exist controversies on their shape, sizes, interdiffusion, etc.... In the following, we discuss QDs that retain a truncated cone shape with a basis angle of 30°, a height h = 2–3 nm and a typical radius R = 10 nm (see Fig. 4). Our calculations, therefore, attempt to describe InAs QDs embedded into a GaAs matrix (or a GaAs/AlAs superlattice). The QD

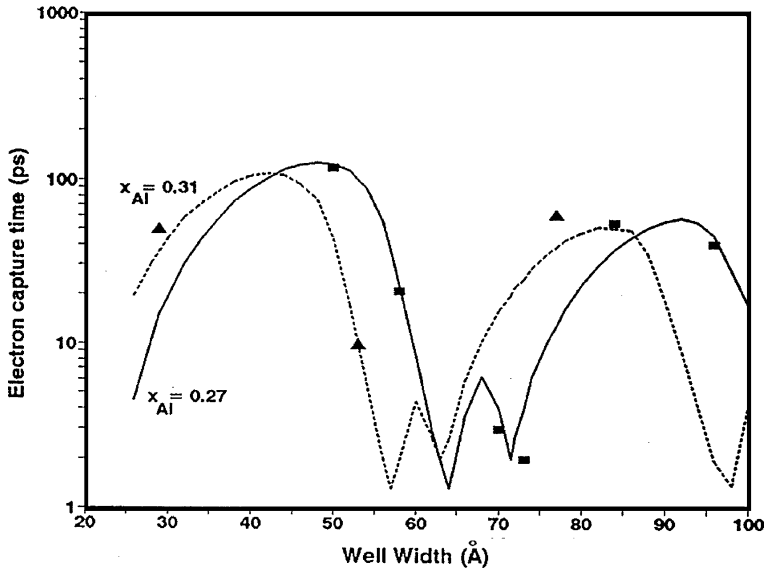

Fig. 3 Theoretical curves of the electron capture time as a function of the well width for x_{Al} = 0.27 and x_{Al} = 0.31. Symbols: experimental capture times for electrons. From [17]

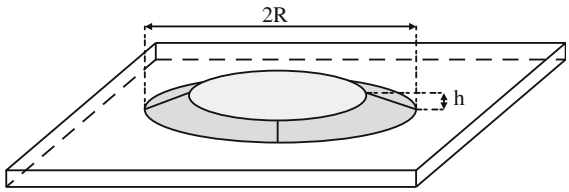

Fig. 4 Schematic representation of an InAs QD

floats on a thin (0.5 nm) wetting layer. Within the one band effective mass model ($m^* = 0.07m_0$), the QD strongly binds two states; one non-degenerate state with S symmetry, which is the ground state, and a twofold degenerate (P_+ and P_-) excited state. A second S state is marginally bound as well as two D_+, D_- states. Here S, $P_\pm$, $D_\pm$ refer to the projection along z of the electron angular momentum in the effective Hamiltonian. Including spin, a dot could therefore load 12 non-interacting electrons. Actually, there are ample evidences by capacitance spectroscopy [19] that InAs QDs can load six electrons. The situation is less clear for the remaining six electrons because the one electron binding of these states is quite shallow making the stability of the multi-electron occupancy of these excited shells a debatable issue. Due to the nanometric sizes of these QDs, there exist large Coulomb effects in QD bound states. Coulomb blockade (or charging) energies have been measured by capacitance techniques [19]. The Coulomb charging energy in the S shell amounts to be about 35 meV. This value is close from the numerical estimates one can make [20]. Figure 5 displays the Coulomb matrix elements for S and $P_\pm$ states [26] in cones versus the basis radius and keeping the basis angle constant (12°).

Besides the purely numerical calculations of the QD bound states, approximate solutions using the variational technique exist that are more flexible and still quite accurate. A numerical/variational method [21, 22] proved useful to handle both single- and multi-stacked dots. It consists in searching the best solutions that are separable in z and ρ and where the ρ dependent wavefunction is a priori given and depends on one or several parameters λ_i. The in-plane average of the Hamiltonian is then taken leaving a one dimensional effective Hamiltonian governing the z dependent part of the wavefunction. Because of the radial averaging procedure, the 1D Hamiltonian depends on the variational parameters λ_i of the radial part of the wavefunction. This Hamiltonian is numerically solved. Its lower eigenvalue is retained and its minimum versus the λ_i is searched. Because the z dependent problem is solved numerically, one gets several eigenvalues besides the lower one. They should in principle not be retained. Note, however, that if the potential energy were the sum of a z-dependent part and of a radial part, the problem would be exactly separable and, for a given radial wavefunction, we would be allowed to retain all the eigenvalues of the effective z-dependent motion. This suggests that if the problem is almost separable, then the excited states solutions of this variational ansatz may correspond to actual states of the real heterostructure. An example [22] of application of the separable method is shown in Fig. 6 for a

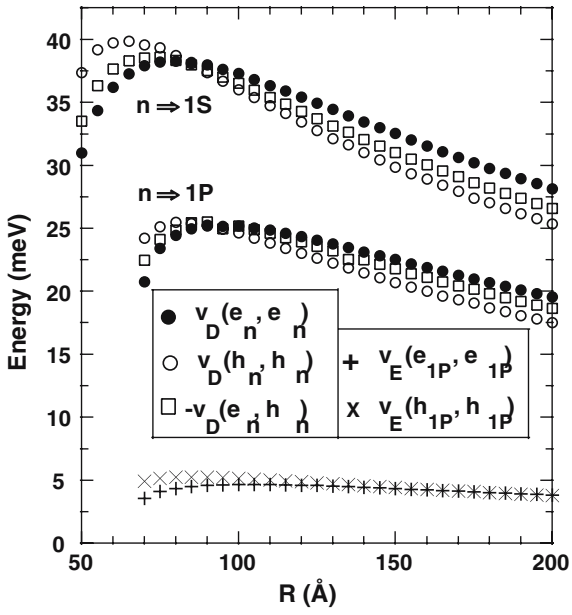

Fig. 5 Coulomb matrix elements for InAs QDs for 1S and 1P states versus dot radius R. Direct: v_D. Exchange: v_E. Cones. $V_e = 0.697$ eV, $V_h = 0.288$ eV. Basis angle: 12°, 0.333 nm thick wetting layer

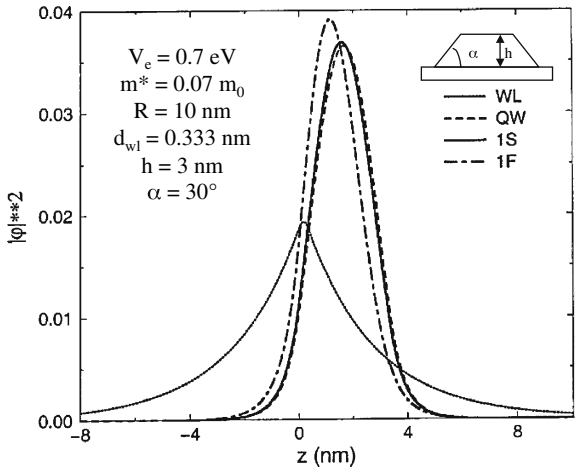

Fig. 6 Square modulus of the envelope functions versus z for different states of an InAs QD. Truncated cone. $V_e = 0.697$ eV, $R = 10$ nm, $h = 3$ nm, basis angle: 30°. 0.333 nm thick wetting layer. From [22]

single QD, where the z- dependent probability densities for the $1S$ and $1P_{\pm}$ states are shown versus z, together with the wetting layer one ($V_b = 0.7$ eV). It is interesting to notice that the z dependent $1S$ and $1P$ probability densities look very much alike, as if the problem were a separable one.

The continuum states of a QD are in general impossible to derive algebraically, except in a few cases (e.g., spherical confinement [23, 24]). So, very often, plane waves were used to describe these states in the numerical calculations. Sometimes, this approximation is not very good because, actually, a QD is a deep (a fraction of an eV) and spatially extended (thousands of unit cells) perturbation.

Capture

The carrier capture by a quantum dot due to the emission of an LO phonon is reminiscent of the capture by a QW. There is however a big difference between them. It is the fact that there exists a whole range of dot parameters where the capture is impossible because of the entirely discrete nature of the QD bound states [24–26]. If there is no bound state within $\hbar\omega_{LO}$ of the edge of the 2D continuum (the wetting layer states) then it is impossible to ensure the energy conservation during the capture process. In QWs instead, each z dependent bound state carries a 2D subband associated with the in plane free motion and any energy difference between QW bound states and the onset of barrier continuum can be accommodated (of course with a decreasing efficiency when increasing the energy distance between the bound state and the onset of the continuum).

When it is energy allowed the carrier capture by a QD is efficient (1–40 ps). When the carrier capture by the emission of one LO phonon proves to be impossible, Magnusdottir et al. [25] showed that the capture due to the emission of two LO phonons comes into play with an efficiency that is not very much reduced compared to that of the one LO process. Magnusdottir [24] also handled the case of one LO phonon capture when the dot is already occupied by one electron or one hole. The outcome of the calculations was that there is little difference on the narrowness of the parameter region that allows a LO phonon-assisted capture. Experimentally, the carrier capture time has been deduced from the analysis of time-resolved photoluminescence experiments on QD ensembles. Auger effect was often invoked to interpret the data. In particular, a very fast electron capture was measured [27] in p-type modulation-doped QDs. Very recently, the transient bleaching of the wetting layer absorption edge was analyzed by Trumm et al. [28]. A fast (3 ps) electron capture time was deduced from the experiments. This time was independent of the density of carriers photoinjected into the wetting layer.

In QDs it is now well established [29] that the energy relaxation among the bound states and due to the emission of LO phonons cannot be handled by the Fermi Golden Rule whereas this approach works very nicely in bulk and QW materials [13]. The coupling to the LO phonon is so strong compared to the width of the continuum (here only the narrow LO phonon continuum since we deal with the QD discrete states) that a strong coupling between the two elementary excitations is established with the formation of polarons. The existence of polarons was confirmed by magneto-optical experiments [30]. Since the QDs may display virtual bound states it is an interesting question to know whether a strong coupling situation could be established between the continuum electron in a virtual bound state and the LO phonons. If it were the case, the notion of capture assisted by the (irreversible) emission of phonons should be reconsidered. To answer this question, Magnusdottir et al. [31] studied the case of a spherical dot that binds only one state ($1s$) while the first excited state $1p$, triply degenerate on account of the spherical symmetry, has just entered into the continuum, thereby producing a sharp resonance near the onset of this continuum. The energy distance between $1s$ and $1p$ was first chosen equal to the energy of the dispersionless LO phonons, in order to maximize the electron–phonon coupling. The calculations of the eigenstates of the coupled electron and phonons reveal that polaron states are indeed formed. In addition, one of the two polarons become bound to the QD while the other is pushed further away in the continuum (see Fig. 7). So, the coupling to the phonons has changed the nature of the electronic spectrum. However, this situation is rather exceptional and as soon as one detunes the electronic energy distance from the phonon, the polarons are quickly washed out.

Very recently, Glanemann et al. [32] studied the phonon-assisted capture in a QD from a 1D wire by quantum kinetics equations and found significant differences from the semiclassical predictions. Particularly, because of the short time scale involved in the capture, the QD population is not a monotonically increasing function of time, even at low temperature where there is no available phonons to de-trap the carrier.

Photo-detection

Since the conduction and valence band discontinuities between QDs and their hosts are usually a fraction of an eV, the QDs are inherently taylored to be used in

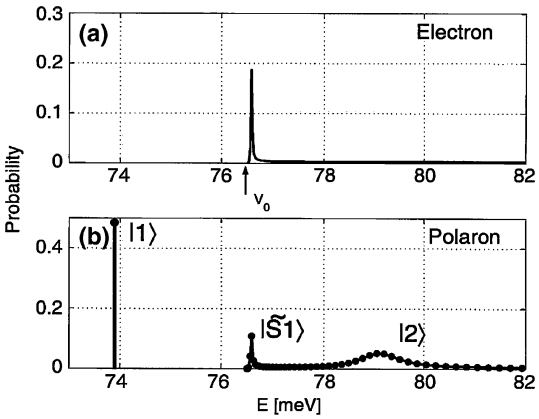

Fig. 7 (**a**) Integrated probability that an electron in a *p* continuum state is found in the QD versus energy *E*. Spherical dot. V_e = 76.49 meV. $m_e = 0.067m_0$. Dot radius: 8.55 nm. R_b = 1500 nm. There is a virtual bound state at 76.58 meV and a true bound state with *S* symmetry at *E* = 41.59 meV. (**b**) Polaron states |1⟩ and |2⟩ that arise from the diagonalization of the Fröhlich Hamiltonian between the *p* continuum and the 1LO phonon replica of the bound *S* state. From [31]

the photo-detection of infrared light, ranging typically from 30 to 400 meV. There have been indeed several studies of photo-detectors based on InAs QDs (see e.g., [33–50])

In addition, the discrete nature of their lower lying eigenstates allows, at first sight, a photo-ionization for normal incidence that should be of the same order of magnitude as the photo-absorption for light propagating in the layer plane with its electric field lined along the *z*-axis. For QW structures, the so-called QWIP devices, only the latter is allowed, forcing the use of waveguide geometry to detect light [51]. Besides, the nature of the QD continuum is largely unexplored and it would be useful to know if there are certain energies in these continuums that influence markedly the photo-absorption. In this respect, Lelong et al. [50] reported a theoretical analysis of Lee et al. data [49] that correlated features of the photo-absorption to the virtual bound states of the QDs. Finally, the link between the QD shape and the nature of the photo-absorption, if any, remains to be elucidated. We shall show that the flatness of actual InAs QDs not only influences the QD bound states but also shapes the QD continuum. In practice, the only continuum states that are significantly dipole-coupled to the QD ground bound state are also quasi-separable in ρ and z and display radial variations in the quantum dot region that resemble the one of a bound state. Also, like in QWs, the $E//z$ bound-to-continuum (B–C) absorption is considerably stronger than the $E//x$ (or y) one. In addition, the $E//z$ B–C QD absorption is almost insensitive to a strong magnetic field applied parallel to the growth axis, in spite of the formation of quasi Landau levels (again like in QWs). All these features point to regarding the photo-absorption of InAs QDs as being qualitatively similar to the QWs one, although there is some room left for recovering a strong $E//x$ (or *y*) B–C photo-absorption, as discussed below.

The structures we shall discuss were grown by MBE and consist of periodic stacks of InAs QD planes embedded into a GaAs/AlAs superlattice [37, 52]. Since the period is small (≈10 nm) the QDs line up vertically, on account of the strain field. The 1 nm thick AlAs layers were Si-doped to load the QDs with one electron on average (see Fig. 8 for a sketch [53]). A comparison was made between QD/GaAs and QD/GaAs/AlAs periodic stacks. The latter devices display better performances due to a significant reduction of the dark current [37, 52]. The QDs are modeled by truncated cones with a height 2 nm, a basis radius *R* = 10.2 nm and a basis angle of 30°. The one electron states were calculated from a numerical diagonalization [52, 53] of the hamiltonian:

$$H = \frac{p^2}{2m^*} + V(\rho, z) + \frac{1}{2}\omega_c L_z + \frac{1}{8}m^*\omega_c^2\rho^2 + \delta V(\vec{r}) \qquad (9)$$

where the magnetic field **B** is taken parallel to *z*, $\omega_c = eB/m^*$, $V(\rho, z)$ is the isotropic part of the QD confining potential and δV any potential energy that would break the rotational invariance around the *z*-axis (e.g., if the QDs have an elliptical basis, if there exist piezo-electric fields,...). The dots are at the center of a large cylinder with radius R_C = 100 nm. Because the confining potential depends periodically on *z*, the eigenstates of *H* can be chosen as Bloch waves labeled by a 1D wavevector k_z with $-\pi/d < k_z \leq \pi/d$. A Fourier–Bessel basis was used at $B = 0$ while at $B > 10$ T we use a Fourier–Landau basis. The conduction band offset between InAs and GaAs (respectively, between GaAs and AlAs) was taken equal to 0.4 eV (1.08 eV) while the effective mass $m^* = 0.07m_0$ as obtained from magneto-optical data [30]. Figure 9

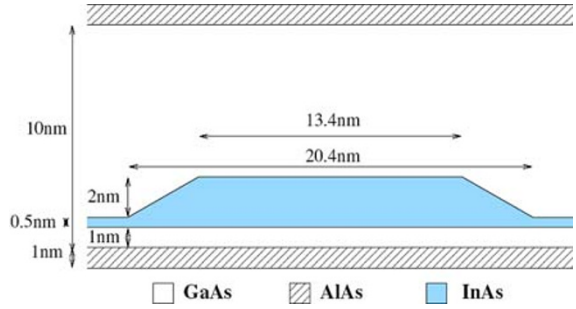

Fig. 8 Schematic representation of the supercell including the dot and its wl. Period *d* = 11 nm. From [53]

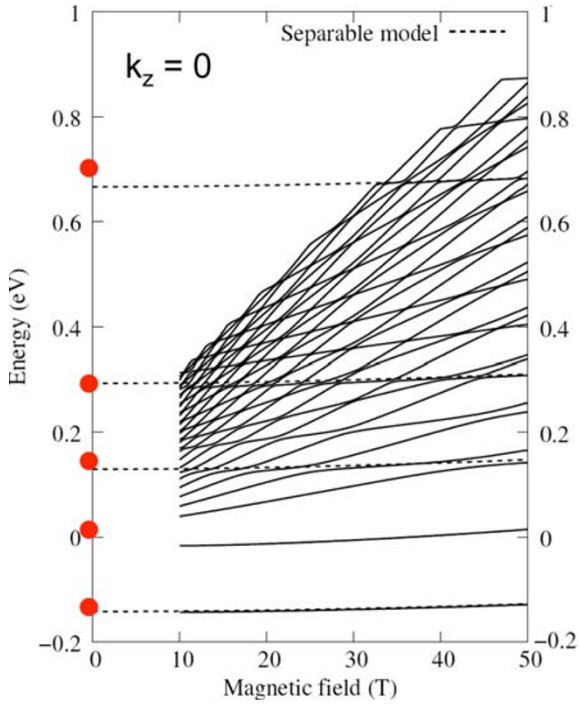

Fig. 9 Calculated energy levels with S symmetry versus magnetic field. The dashed lines are the results of the separable model with a Gaussian radial function. $k_z = 0$. From [53]

shows the calculated Landau levels with S symmetry of a GaAs/AlAs/QD superlattice versus $B \geq 10$ T at $k_z = 0$. The extrapolation of the fan chart to $B = 0$ are marked by circles. They are roughly: 16 meV, 144 meV, 293 meV and 701 meV. Two states with S symmetry and a negative energy do not belong to a fan. These are in fact the two ($1S$ and $2S$) bound states of a single dot that are very little affected by the periodic stacking. The dashed lines are the results obtained from the separable model with a Gaussian variational wavefunction for the in-plane motion. It is quite remarkable that the $B = 0$ solutions of the effective 1D Hamiltonian are so close from the numerical data not only for the ground state but also for all the excited solutions in the continuum with S symmetry. In principle only the lowest eigenvalue (the ground energy) should be retained in the variationnal approach. All the excited states (for the z motion since the in-plane motion is locked to the best Gaussian for the ground state) are a priori spurious: the Hilbert space retained in the ansatz may be too small to correctly describe the excited states. However, if the problem were separable in z and ρ, all the different solutions for the z motion would be acceptable. The fact that the variational approach works so well suggests strongly that the problem is quasi-separable. In fact, it is the flatness of the dots that leads to the quasi-separability. Since the InAs dots are so flat ($h \ll R$), any admixture between different z dependent wavefunctions costs a very large amount of kinetic energy and, in practice, all the low lying states, bound or unbound, display similar z dependencies.

There are, however, distinct signatures of the non-separability in the $B \neq 0$ spectrum in Fig. 9. In a truly separable problem, the Landau levels of two distinct $B = 0$ edges E_l and $E_{l'}$ for the z motion should cross at fields B such that:

$$n\hbar\omega_c + E_l = n'\hbar\omega_c + E_{l'} \tag{10}$$

The non-separability replaces the crossings by anti-crossings. They are quite small (the lowest anti-crossing in Fig. 9 that shows up near $B = 40$ T is only a few meVs wide and certainly much smaller than the separable terms (about 150 meV). Hence, even for the continuum states, one can conclude that the small aspect ratio of the InAs QDs ($h/R \approx 0.2$) influences most strongly the energy spectrum.

Let us now attempt to quantify the effect of the QD on the energy spectrum of a GaAs/AlAs/InAs(wl) superlattice in which the InAs dot has been removed but all the other parameters remain the same as before. This 1D superlattice has its first miniband that starts at ≈19 meV. The other $k_z = 0$ edges are located at 151 meV, 293 meV and 699 meV. The appearance of low lying bound states and the red shift of the first excited state witnesses the presence of the attractive QD. Conversely, the superlattice effect deeply reshapes the QD continuum. Without superlattice, the onset of the continuum for an isolated dot would be at – 15 meV (edge of the narrow wetting layer QW); with the superlattice it is blue-shifted at +16 meV. Therefore, it is in general impossible to disentangle the QD effects from the superlattice effects. In no case can one assume that one effect is a perturbation compared to the other.

The optical absorption from the ground state $|1S; k_z\rangle$ to the excited states (bound or unbound) $|nL; k_z\rangle$ can now be calculated using:

$$\alpha(\omega) \propto \sum_{nL;k_z} \left|\left\langle \psi_{nL;k_z} \middle| \vec{\varepsilon}.\left(\vec{p} + e\vec{A}_0\right) \middle| \psi_{1S;k_z} \right\rangle\right|^2 \delta\left(E_{nL;k_z} - E_{1S;k_z} - \hbar\omega\right) \tag{11}$$

where $L = S, P_{\pm}, ..., \mathbf{A}_0$ is the vector potential of the static field and ε the polarization vector of the electromagnetic wave. We have only retained the vertical transitions in the first Brillouin zone. In z polarization and within the decoupled model, we expect that the only non-vanishing excited states probed by light are

the $L = S$ states shown in Fig. 9. This expectation is fully supported by the full calculation as shown in Fig. 10. The main difference between the full calculation and the predictions of the separable model is the double peak that appears near 0.26 eV at $B = 35$ T. It is a consequence of the anti-crossing discussed previously. Quite striking is the insensitivity of the absorption spectra to the magnetic field. It is reminiscent of the QW behavior, where it is known that, besides band non-parabolicity, the intersubband spectrum should in an ideal material be B-independent for z polarized light.

It was thought that QDs could lead to infrared absorption for x or y polarized light while QWs respond only to z polarization. Actually, this expectation is frustrated by the lateral size of regular dots ($R \approx 10$ nm) which allows several states of different L to be bound. Hence, all the oscillator strength for the x polarization is concentrated on the bound-to-bound S–P transition that takes place near 50 meV. Very little is left for the S-to-continuum (P) transitions and the photodetection in this polarization is not efficient. A way to remedy this drawback is to push the ground P states in the continuum, transforming them into virtual bound states (Note that the flatness of the QDs makes the virtual bound state for the z motion to occur at very high energy). This takes place for $R \approx 5.8$ nm. An example of the drastic changes in the oscillator strength for x polarization is shown in Fig. 11 at $B = 0$ and $k_z = 0$ between S and P levels in dots with decreasing radius. Starting from a large dot ($R = 7$ nm) where the P level is bound and exhausts all the oscillator strength, the QD radius decreases down to 4.5 nm leading to a broadened peak in the continuum whose amplitude decreases with increasing energy in the continuum.

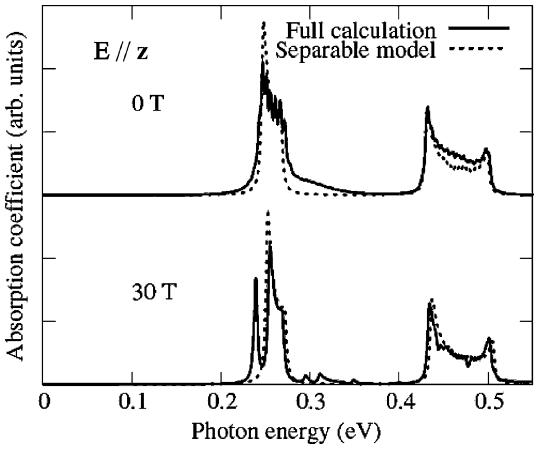

Fig. 10 Absorption coefficients versus photon energy at $B = 0$ and $B = 30$ T calculated by two models for $\varepsilon//z$. From [53]

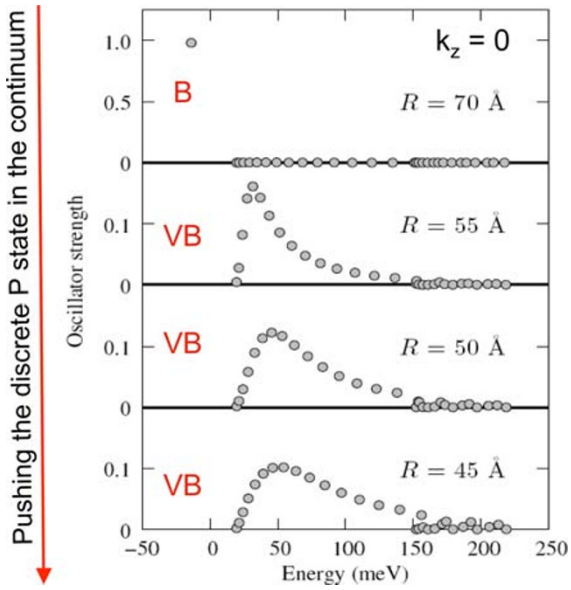

Fig. 11 Oscillator strength versus transition energy from the ground S state to the first 30 P states at $B = 0$, $k_z = 0$ and for several basis radius. $\varepsilon//x$. The ordinate in the case $R = 70$ Å is five times bigger than the others. From [53]

To conclude this section, we show in Fig. 12 a comparison between the calculated and measured absorption in GaAs/AlAs/QD superlattices for z polarization [52]. It

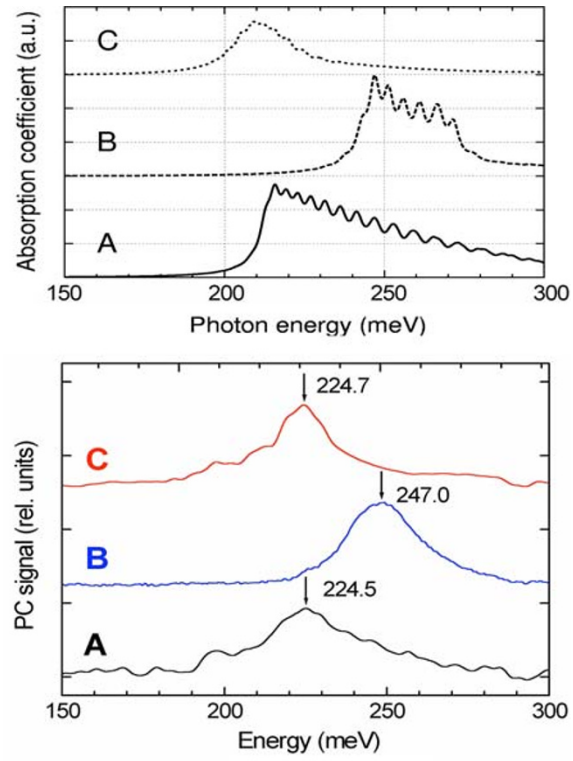

Fig. 12 Comparison between the calculated absorption spectra and measured photoconductivity spectra of InAs QDs versus photon energy. Adapted from [21] and [52, 53]

is seen that a reasonably good description of the experimental absorption is obtained by the calculations, despite our neglect of the inhomogeneous broadening due to fluctuating R from dot to dot. This is probably due to the fact that the ideal spectra are already very broad due to the large energy dispersion of the final states.

In summary, it appears that the continuum of the QDs, which plays a decisive part in the light absorption, depends sensitively on the surrounding of the dots (the superlattice effect). However, the photo-response is deeply affected by the flatness of these objects, to a point that most of the infrared absorption features look very much the same as those found in QW structures, except if special QD parameters are carefully designed.

Two particle continuum states in QDs

In QDs, one often deals with many particle states: even in a single undoped QD the radiative recombination involves at least one electron–hole pair. When several particles come into play, one should wonder about their excited states. It may very well happen that the energy of a *discrete excited* two particle state lays inside a *mixed continuum* of states that corresponds to a situation where one of the two particle lays in a lower state (possibly the ground state) while the other has been ejected in the continuum. A well known example of such a feature occurs in He atoms for the doubly excited $2P$–$2P$ discrete state whose energy is larger than the mixed bound-continuum states formed by keeping one electron in a $1S$ orbital while the other belongs to the continuum. It is our implicit use of one particle picture that often leads us to the wrong conclusion that the product of two discrete states should necessarily belong to the discrete part of the two particles spectrum.

Two particles effects are important for the capture/ejection of one carrier inside/outside a QD. They are therefore the agent that links the QDs bound states, with their inherently low number, to the macroscopic outside world with its huge phase space. So, the two particle effects can be either beneficial by bringing carriers where we want to see them but also detrimental in that they may lead to a loss of carriers bound to the dots. Another detrimental effect, important in view of the quantum control of the QD state, imperatively needed to any kind of quantum computation, arises if a coupling is established between the QD bound states and their environment (see e.g., [54, 55]). The environment is essentially decoherent: its density matrix is diagonal with Boltzmann-like diagonal terms and any off diagonal term decays in an arbitrarily short amount of time. There is, therefore, a risk of polluting the quantum control of the QD if two particle effects come into play and connect the QD bound state to the continuum of unbound QD states. Let us recall that, as mentioned earlier, there are both a 2D continuum associated with the wetting layer states and a 3D one associated with the surrounding matrix.

The carriers interact because of Coulomb interaction. The capture or ejection of particles due to Coulomb scattering between them is usually termed Auger effect.

Two particle effects involve either different particles, like electrons and holes, or two identical particles, e.g., two electrons. In the latter situation, the wavefunction should be anti-symmetrized to comply with the Pauli principle.

Electron–hole Coulomb scattering

The electron capture to a QD by scattering on delocalized holes has been investigated by Uskov et al. [56] and Magnusdottir et al. [57] assuming unscreened Coulomb scattering and conical, spherical or pancake-like QD shapes. These authors found a quadratic dependence of the scattering rate upon the hole carrier concentration: if R is the rate of carriers making a transition from the wetting layer to the QD bound state, the numerical results can be described by:

$$R = C_{\mathrm{eh}} p_{\mathrm{h}}^2 \tag{12}$$

where p_{h} denotes the hole concentration and C_{eh} is a constant. In contrast to the single carrier capture due to LO phonon emission (see above), the Coulomb scattering is always allowed. It is the more efficient when the momentum change for the carrier that remains delocalized (here the hole) is the smaller. If one assumes a Boltzmann distribution of the continuum states, then the Auger capture of an electron to a QD will be the more efficient when there is an electronic level close from the onset of the continuum. Values of C_{eh} reach 10^{-23} m^4 s^{-1}. They are typically two orders of magnitude smaller than the Auger rate of electron capture by electron–electron scattering. This can be understood as follows: the holes have a larger mass than the electrons. Therefore, for a given excess energy, the scattered hole will undergo a larger change of wavevector than would a scattered electron. This implies that the Coulomb matrix elements that show up in the Fermi Golden Rule will be smaller for holes, in particular the form factors (for a more thorough analysis, see [24]). The same reasoning leads to the

conclusion that, for given QD parameters, the capture on a P_e level should be more efficient than on S_e level.

It is also possible that the Auger scattering by delocalized holes leads to a relaxation of electrons that are already bound to the QDs in excited states. This relaxation mechanism was first studied by Bockelmann and Egeler [58]. Like the electron capture by Auger effect, its efficiency increases linearly with the hole concentration. It was found that a fast relaxation (say a transition rate for relaxation in excess of 10^{11} s^{-1}) was possible at relatively large hole concentration (say $p_h > 10^{11}$ cm^{-2}) and also that the numerical results are little affected by using unscreened or dynamically screened coulombic potentials.

It has been suggested by Efros et al. [59] that electron–hole scattering between bound states could lead to an electron relaxation accompanied by a simultaneous ''heating'' of the hole. Strictly speaking this relaxation does not take place: if the electron–hole pair possesses only discrete energy levels, then either it has been placed initially in one of these states and then nothing happens, or it has been prepared in a linear superposition of these states and then, the pair will visit all its (finite number of) available states. In particular, as time flows, it will come close in energy (or even coincides with) the initial states (quantum resurgence). The electron relaxation cannot be irreversible because there is no continuum to create this irreversibility. However, it may well happen that in practice the excited hole levels (because of the hole heavy effective mass or the particular shape of the dot) are so dense that they actually mimic a continuum. This question clearly requires further studies, taking in particular into account the fact that irreversible acoustical phonon emission becomes efficient between closely spaced discrete levels [60].

Irreversible Auger relaxation accompanied by the ejection of the hole is possible if the initial energy of the electron–hole pair exceeds the energy of the pair where the electron has a lower energy and the hole is in the continuum (either 2D or 3D). This phenomenon was discussed by Ferreira et al. [26] and shown to be very efficient when it is energetically allowed. It is therefore beneficial for the relaxation. We shall now see that it is intimately linked to debated experimental findings.

It has been shown by Toda et al. [61], and since observed by many groups [62–65], that continuums of optical absorption existed in InAs QDs at much lower energy than expected for the onset of the wetting layer-wetting layer transitions (labeled w_e–w_h in the following) but at larger energy than the ground recombination line (S_e–S_h). In the following, we assume cylindrical symmetry for QDs and label electron–hole states by indexing the one particle states by e or h. Figure 13 shows a single dot photoluminescence excitation spectrum versus the excess electron–hole energy compared to S_e–S_h. It is seen that for excess energies > 50 meV, there exists peaks that are superimposed to an increasing background. It is noteworthy that the width of these peaks increases with increasing excess energy.

Complementary information were obtained from the study of the temperature dependence of the peak widths in different single InAs QDs by Kammerer et al. [63] (see Fig. 14). Compared to Oulton et al. [64], these dots support less bound states, in other words P_e–P_h is closer from w_e–w_h, the onset of the 2D continuum (≈ 66 meV compared to ≈ 195 meV). It was found that the peak widths increase continuously with T and, like in Oulton et al's experiments, that the excited peak

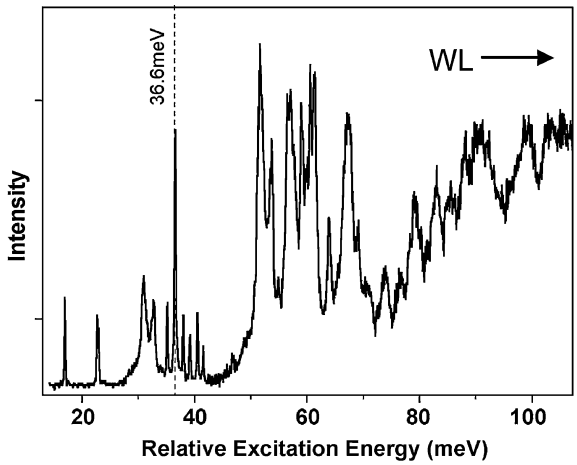

Fig. 13 Photoluminescence excitation spectrum of a single InAs/GaAs QD versus the energy of the incident light measured from the photoluminescence line. Courtesy Dr. R. Oulton

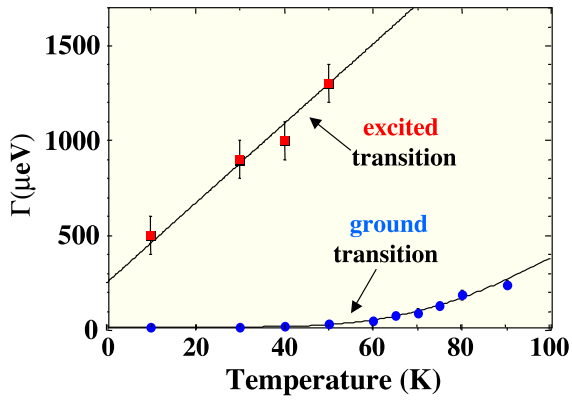

Fig. 14 Full width at half maximum of the ground transition and of an excited transition in a single InAs QD versus temperature. Adapted from [61]

(attributed to P_e–P_h) displays larger widths than the ground one (S_e–S_h). More striking is the faster temperature increase for P_e–P_h compared to S_e–S_h. Actually, it appears that $P_e - P_h$ has a width that increases linearly with T, a feature that recalls what is usually observed in bulk materials or QW structures. In addition, the order of magnitude of the slope of this linear increase is comparable to the findings in QW structures. In the latter, the linear increase in the line broadening is simply due to the number of acoustical phonons $n(T)$ that are irreversibly emitted by the QW or bulk excitons: at high temperature $n(T)$ becomes proportional to T. This phonon emission is accompanied by an energy relaxation of the exciton, through its translational kinetic energy, till a (very small) wavevector where the emission of acoustical phonons becomes impossible. The fact that the same feature shows up in QDs, believed to display only discrete states, was puzzling. In QDs, there is a priori no e–h continuum that surrounds the discrete S_e–S_h or P_e–P_h discrete lines. Hence, the only possible acoustical phonon emission would be due to either the electron or the hole of the pair relaxing towards a lower state. This relaxation is however known to be very inefficient (phonon bottleneck) as soon as the energy difference between the two levels exceeds a few meVs [60, 66]. The puzzle was resolved by Vasanelli et al. [67] who pointed out that, if P_e–P_h has a larger energy than the mixed (or crossed) continuum generated by letting the electron to occupy a lower state (e.g., S_e) in lieu of P_e while the hole would be kicked out from the QD, then it will auto-ionize due to Coulomb interaction. Symmetrically, the hole could relax while the electron would be ejected from the QD. With the usual InAs/GaAs QDs, it is the former mixed continuum that has the lower energy.

Let us briefly see how the discrete state P_e–P_h acquires a finite lifetime because it is Coulomb-coupled to one (or several) continuum(s) (for details see [22]). To simplify the matter as much as possible, we retain only P_e–P_h as the only discrete state of the problem. Further, we take only one mixed continuum into account. Since the diagonal Coulomb matrix elements are quite large, we write:

$$H = H_e + H_h + \delta|P_eP_h\rangle\langle P_eP_h| + (V_{eh} - \delta|P_eP_h\rangle\langle P_eP_h|) \quad (13)$$

where $\delta = \langle P_e\, P_h\, |V_{eh}|\, P_e\, P_h\, \rangle$ and V_{eh} is the electron–hole Coulomb coupling. The discrete state is at the same energy as the S_e–w_h continuum. Then, its lifetime is given by the expression:

$$\frac{\hbar}{2\pi\tau_{P_e-P_h}} = \sum_{\nu_h} |\langle P_eP_h|V_{eh}|S_e\nu_h\rangle|^2 \delta\left(\varepsilon_{P_{e_{P_h}}} - \varepsilon_{S_e\nu_h}\right) \quad (14)$$

In the previous equation, the matrix elements are difficult to evaluate because they involve the exact continuum states of the hole $|\,\nu_h\rangle$. If one approximates these states by the plane waves $\left|\vec{k}_h\right\rangle$, the evaluation of the matrix elements becomes simple and for typical dots with $m_e = 0.07m_0$, $m_h = 0.38m_0$ and using the variational solutions [21, 22] for the P_e, S_e, P_h states, we get a lifetime in the range of 1–100 ps for the P_e–P_h transition, depending on the QD radius. Note that this is considerably shorter than the radiative lifetime ($\approx$ 1 ns). The auto-ionization lifetime does not vary much with increasing P_e–P_h energy because the continuum to which P_e–P_h is superimposed is 2D. However, like in the Auger capture, the trend for τ is towards an increase (i.e., a decreasing linewidth of the P_e–P_h line) with increasing detuning of the P_e–P_h transition from the onset of the continuum: the ejected electron has an increasing kinetic energy and therefore its Coulomb matrix elements are smaller. The decreasing trend would be more pronounced if it were the hole that was ejected from the dot.

Within the auto-ionization formalism one readily understands the experimental observations [63, 64] that the width of the discrete peaks superimposed to the increasingly larger continuum was increasing. It is simply that further and further crossed transitions channels open when the e–h pair energy increases.

The net result of the Coulomb coupling is that the e–h pair spectrum becomes continuous around the discrete state. Hence, it becomes possible to envision that the now virtual bound P_e–P_h state becomes coupled to other states of the continuum by the emission of acoustical phonon of low energy (1 meV or so). The coupling to the phonons is the sum of the electron coupling and of the hole coupling. The emission or absorption of a phonon is therefore due to one particle, the other being a spectator. Because there is no common state to P_e–P_h, and S_e–ν_h, we see that there is no direct phonon coupling between the discrete state P_eP_h and the continuum. To get a non-zero term (see Fig. 15), one should Coulomb admix P_e–P_h with X_e–ν_h or S_e–X_h, where X_e, X_h are two arbitrary electron or hole states. The larger admixture is provided by S_e–S_h. Hence:

$$|\psi\rangle \approx |P_eP_h\rangle + \tfrac{1}{\Delta}|S_eS_h\rangle;$$
$$\Delta = \varepsilon_{P_e} - \varepsilon_{S_e} + \varepsilon_{p_h} - \varepsilon_{S_h} + \langle P_eP_h|V_{eh}|P_eP_h\rangle - \langle S_eS_h|V_{eh}|S_eS_h\rangle \quad (15)$$

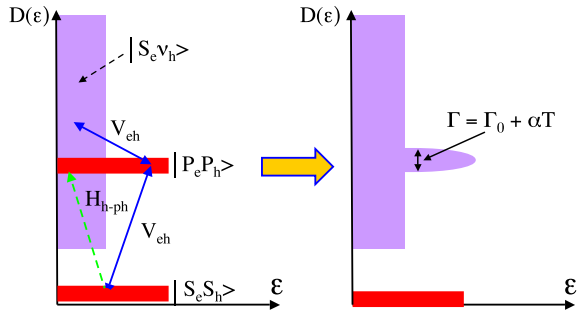

Fig. 15 Sketch of the perturbation schemes that contribute to the Auger or phonon broadening of an excited transition (here P_e–P_h) superimposed to a crossed continuum (here S_e–ν_h)

The lifetime limited by the acoustical phonon emission is therefore given by:

$$\frac{\hbar}{2\pi\tau_{em}} \approx \sum_{\nu_h}\sum_{\vec{Q}} \left|\alpha_{ac}\left(\vec{Q}\right)\right|^2 \frac{\left|\langle S_h|e^{-i\vec{Q}.\vec{r}_h}|\nu_h\rangle\right|^2}{\Delta^2}\left(1+n_{\vec{Q}}\right)$$
$$\delta[F(\nu_h,Q)]F(\nu_h,Q) = \varepsilon_{P_e} + \varepsilon_{P_h} + \langle P_eP_h|V_{eh}|P_eP_h\rangle - (V_{bh} + \varepsilon_{\nu_h} + \varepsilon_{S_e} + \hbar c_S Q) \quad (16)$$

where **Q** is the 3d phonon wavevector and bulk isotropic phonons have been considered. $n_{\mathbf{Q}}$ is the Bose-Einstein occupation number and c_S the sound velocity. α_{ac} is the hole-acoustical phonon interaction and V_{bh} is the height of the QD potential for holes and ε_{ν_h} is the kinetic energy of the ejected hole. A similar expression holds for phonon absorption except that $1 + n_Q$ should be replaced by n_Q. The linear increase of the broadening with T follows immediately since at large T the number of acoustical phonons $n_Q \approx k_BT/\hbar\omega_{\mathbf{Q}} \gg 1$. Likewise the Auger broadening, we expect the phonon broadening to increase with increasing energy of the auto-ionizing state. This is because of the multiplication of the crossed continuums and hence of the larger density of final states for the phonon emission. One finds that the slope of the P_e–P_h linewidth versus T is a few tens of μeV/K for typical QDs.

In summary, the existence of mixed continuum allows us to write that:

$$\frac{1}{\tau} = \frac{1}{\tau_c} + \gamma T \quad (17)$$

where τ_c is the lifetime limited by Coulomb effects with the further information that both $1/\tau_c$ and γ increase if one investigates states that are more excited than P_e–P_h.

At elevated temperature optical phonon scattering would come into play. In contrast with acoustical phonons, the coupling with LO phonons does not follow the Fermi Golden Rule but rather gives rise to mixed elementary excitations: the polarons [68, 69]. The previous weak coupling description is inappropriate to handle the auto-ionization of the P_e–P_h polaron. Work remains to be done in this area.

Note that it is nowadays experimentally well established that acoustical phonons dress the Coulomb correlated e–h pairs (as witnessed by the pedestal that supports the sharp zero phonon line [70], observed in the interband spectroscopy of single QDs). Thus, one may wonder if the non-perturbative couplings [71] that lead to these pedestals should not be taken into account in the calculation of the phonon-assisted lifetime of P_e–P_h or more excited transitions. Actually, we do not believe this is the case because the physical mechanism at stake, the acoustical phonon emission by a bound electron–hole pair to become a mixed continuum state, is genuinely outside the scope of the formalism that leads to the pedestal. The latter is based on the restriction of the electron–hole pair Hilbert space to a single level.

The irreversible emission of acoustical phonons and the Auger disintegration of the excited e–h pairs share irreversibility in common. The size of the continuum to which the initial discrete state is coupled is so big that the probability that the system returns to its initial quantum state decays exponentially to zero with a short time constant (a few ps). This irreversible decay affects not only the populations of the P_e–P_h levels but also the coherences of the P_e–P_h interband transition. At the largest, the lifetime of the coherence of this excited transition is twice the population lifetime. Therefore, any entanglement one can imagine which would involve the excited pair state is prone to a ps decay if the discrete pair state has a larger energy than the first mixed continuum.

Coulomb scattering between identical particles

As mentioned above, the main difference between the Coulomb scattering of identical particles compared to that of unlike particles is the requirement of anti-symmetrization. Bockelmann and Egeler [58] studied the relaxation of an already bound electron to a QD by Auger effect with a plasma of delocalized electrons. They found this Auger relaxation to become efficient (transition rate in excess of 10^{11} s^{-1}) only for large plasma concentration (10^{11} cm^{-2}). A similar calculation was undertaken by Wetzler et al. [72] who studied the case of Auger processes between the electrons bound to a QD and 2D (electrons in a wetting layer, a nearby QW) or 3D (contacts) delocalized carriers located a

distance d from the QD plane. For a 2D density of 10^{11} cm^{-2} mobile carriers located at $d = 0$ nm from the QD plane, Wetzler et al. found a 10^{12} s^{-1} transition rate for a 30 meV energy variation of the bound carrier. The rate increases linearly with the carrier concentration. If, however, the 2D gas is at $d = 40$ nm away from the QD plane, the Auger rate drops to 10^{8} s^{-1} at $T = 77$ K and a 2D carrier concentration of 10^{11} cm^{-2}.

Uskov et al. [56], Magnusdottir et al. [57] studied the Auger capture from a 2D electron plasma (or a hole plasma). They found a capture rate that grows quadratically with the carrier concentration (Fig. 16). Again only carrier concentration in excess of 10^{11} cm^{-2} leads to significant rates. Also, the capture is the more efficient to the shallower bound state because of as maller wavevector transfer to the scattered particle. Auger scattering and capture were also studied theoretically by Nielsen et al. [73], Nilsson et al. [74] and by Chaney et al. [75].

Because of its technological importance for lasers, the Auger rates in QD were measured by several groups [76–82]; for a general discussion see [83]). Marko et al. [84] recently demonstrated that the Auger recombination remains an important factor in 1.3μm InAs QD lasers while it plays a less important role in QD lasers that emit at 980 nm. In the 1.3 μm case the threshold current increases with temperature while it remains constant in the 980 nm case, as indeed expected from lasing action between discrete levels.

When two electrons are bound to a QD, in a P_e shell for instance, very short relaxation times (ps) for one electron to S_e were calculated by Ferreira et al. [26].

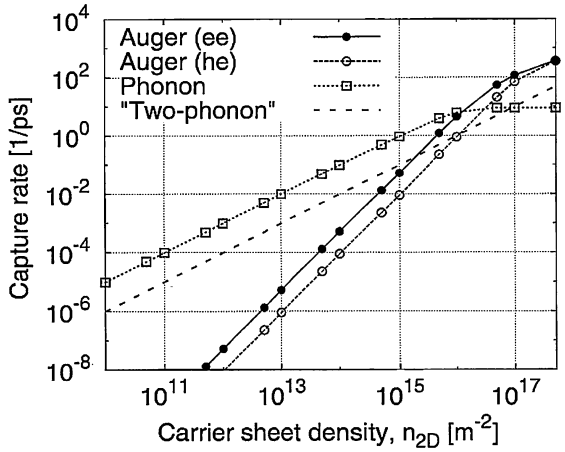

Fig. 16 The carrier capture rate of electrons into a QD (1*P* state) is plotted versus the carrier sheet density in the wetting layer for LO phonon-assisted and Auger captures. The QD is a truncated cone with $R = 5.4$ nm, $h = 3$ nm and a basis angle of 30°. Courtesy Dr. I. Magnusdottir [24]

This intra dot Auger relaxation occurs only if the initial energy is greater than the onset of the crossed continuum S_e–w_e. It efficiency can be qualitatively understood by noting that it corresponds to a charge of – 2e squeezed in a nanometric volume (a truncated cone with $R = 10$ nm, $h = 2$–3 nm and a basis angle of 30°) and therefore to a large electron 3D concentration.

A series of single dot photoluminescence experiments have been undertaken by Warburton et al. on InAs QDs with a controllable number of electrons [85] and Urbaszek et al. [86]. This control was achieved by placing the QD plane in the intrinsic part of a MIS structure [87]. The ground luminescence line (S_e–S_h) was then observed when the QD is loaded by 0, 1, 2, 3... electrons. Let us first consider the radiative recombination of the doubly charged exciton X^{2-}. It comprises three electrons and one hole. The ground configuration of this complex has the hole in the S_h state. The S_e shell is filled with two electrons. There is one electron in the P_e shell. After optical recombination, no hole is left, one electron is in S_e while the other is in the P_e state. There are two possible two electron states corresponding to a total spin $\sum = 0$ or $\sum = 1$. The $\sum = 0$ state lays at higher energy than the triplet state. The interband transition occurs at lower energy and is considerably broader when the final state is the singlet: broadenings of 0.5 meV and < 0.05 meV for final $\sum = 0$ and $\sum = 1$ states, respectively. Both of these linewidths grow quickly and almost linearly with temperature. These features are reminiscent of the Auger broadening discussed above for the auto-ionization of the P_e–P_h two particle states. However, the intra dot Auger mechanism applies to the X^{2-} case only if both the $\sum = 0$ and $\sum = 1$ (S_e–P_e) energies are above the S_e–w_e edges, i.e.

$$\varepsilon_{P_e} + C_{S_eP_e} \pm \mathrm{Ex}_{S_eP_e} > V_e - \varepsilon_{wl} \tag{18}$$

where C_{S_e} P_e and Ex_{S_e} P_e stand for the direct and exchange Coulomb integrals, respectively, between S_e and P_e electrons, the plus (minus) sign is for the $\sum = 0 (\sum = 1)$ state. V_e is the conduction band offset and ε_{wl} is the energy distance between the bound state for the z motion in the wetting layer and the GaAs continuum. The Coulomb effects between the S_e electron and the electron in the wetting layer has been neglected. The condition given by Eq. (18) is difficult to fulfill in the general case. It was argued [86] that the broadening of the X^{2-} lines and particularly of the $\sum = 0$ one was due to the overlap between these discrete states and the band tail of the S_e–w_e edge due to the shallow binding of the S_e–P_e configuration. Within

this scheme, the very different linewidths of the triplet and singlet state would arise from the different matrix elements between the singlet or triplet states and the bandtail.

Another interesting situation arises when there are three electrons residing in the dot at equilibrium. By adding one electron–hole pair, one finds one hole in S_h state. The S_e shell is filled by two electrons. The P_e shell contains two electrons. Assume the total electron spin $\sum$ is one. This $\sum = 1$ is the initial, discrete, state of the optical recombination (Fig. 17). The final state of the recombination consists in a dot with no hole, one electron in the S_e shell and two electrons in the P_e shell. These three electrons can have a total spin of either $\sum = 3/2$ or $\sum = 1/2$. In Warburton et al.'s and Urbaszek et al.s' experiments, this excited configuration of the QD charged by three electrons was probably degenerate with the continuum of states corresponding to a dot loaded by two electrons both in the S_e shell, the third electron having been ejected in the wetting layer continuum (a $\sum = 1/2$ state). Hence, the $\sum = 1/2$ recombination line, instead of being discrete (or rather displaying a μ eV width due to the radiative broadening), displays a finite width controlled by the Auger effect. This width is of the order of ≈1 meV, in agreement with theoretical estimates [22, 26, 88]. The $\sum = 3/2$ line is much less broad than the $\sum = 1/2$ line because in addition to the Coulomb scattering, an extra spin flip is needed to allow a $\sum = 3/2$ state to disintegrate into a $\sum = 1/2$ continuum.

Furthermore, the PL experiments on charged single dots were undertaken in the presence of a strong magnetic field applied parallel to the growth axis. This strong field Landau quantizes the in-plane motion of the ejected electron. If the Landau quantization is larger than the homogeneous broadening, then the irreversible auto-ionization of the excited configuration (due to Auger effect) becomes suppressed. There are now discrete (but degenerate) wetting layer states. Only a small number of them are Coulomb-coupled to the discrete states, on account of the conservation of the total angular momentum. Any time the magnetic field lines up the energy of the discrete states with one of these wetting layer Landau levels, an anti-crossing takes place and one observes several recombination lines instead of a single one.

Finally, by biasing the structure even further, the wetting layer (assumed empty in the previous discussion) starts to fill. The X^{3-} exciton, $\sum = 1/2$ becomes degenerate with a Fermi sea and complicated many body effects may show up. In one of them, the QD spin becomes screened by Fermi sea at low temperature. The total spin of the Fermi sea plus the QD is zero (Kondo exciton [89, 90]). This is a non-perturbative effect of the Coulomb interaction (in contrast to the Auger decay previously discussed). Smith et al. [91] obtained evidences of spin flip scatterings between the electron bound to a QD and the adjacent Fermi sea in the back contact of a biased QD by observing the change of dark QD bound excitons into bright excitons.

Conclusions

The semiconductor heterostructures of low dimensionality are characterized by a very small number of available quantum states at low energies. This is certainly beneficial if one attempts a quantum control of physical properties that depend sensitively on these sparse states. On the other hand, this makes their direct excitation extremely difficult to achieve. One is then forced to supply these nanometric objects with carriers through their macroscopic surrounding. Certain states of the continuum are better suited than others to play this part; these are the virtual bound states (of a QW, a QD). There are evidences that the virtual bound states control the feeding of the low laying states in a QW. The photoconductive properties of QDs have already evidenced the part played by the virtual bound states.

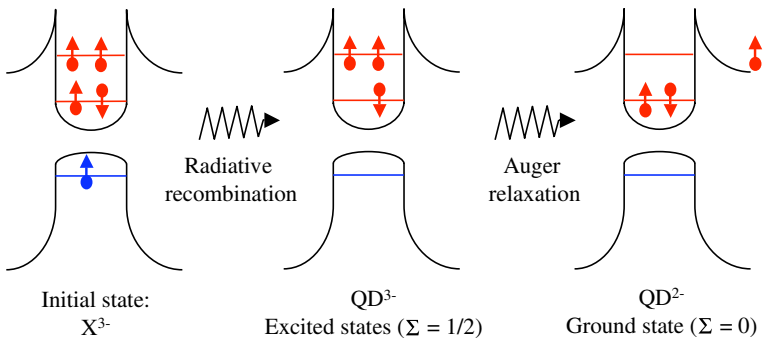

Fig. 17 Sketch of the different charge configurations involved in the radiative recombination of the X^{3-} exciton in a QD

The two particle states are a very rich area to investigate. Any kind of interband optical properties involve electron–hole pairs. Their spectrum can display mixed continuums where one of the particles is bound to the dot while the other travels freely in the wetting layer. These mixed continuums can overlap discrete excited pair states, transforming them into virtual bound states of the pair Hamiltonian. The detrimental action of these mixed continuums on the linewidth of QD excited transitions has been experimentally demonstrated but should receive more attention.

Finally, the electrical control of the loading of a single dot has allowed for the observation of the Auger relaxation of excited configurations of charged QDs when the wetting layer was empty. The coherent mixing of discrete QD bound states with an occupied wetting layer remains, so far, a tantalizing concept.

Acknowledgments The LPA-ENS is ''Laboratoire associé au CNRS et aux Universités Pierre et Marie Curie et Denis Diderot''. One of us (GB) would like to thank Profs. H. Sakaki, Y. Arakawa and K. Hirakawa for their hospitality at the IIS-Tokyo where part of this review was written and for enlightening discussions. A number of colleagues have helped us to investigate more thoroughly the QD continuum. We acknowledge Profs. Y. Guldner, G. Strasser and K. Unterrainer, Drs. G. Cassabois, S. Hameau, N. Regnault, Ph. Roussignol and L.A. de Vaulchier for numerous insights on InAs QDs. We are much indebted to Drs. I. Favero, C. Kammerer, Ph. Lelong, A. Vasanelli, I. Magnusdottir, O. Verzelen, N. D. Phuong, R. Oulton and F. F. Schrey for their active participation to the work reported here.

References

1. D. Bimberg, M. Grundmann, N.N. Ledentsov, *Quantum Dot Heterostructures* (John Wiley and Sons, New York, 1999)
2. O. Stier, M. Grundmann, D. Bimberg. Phys. Rev. B59, 5688 (1999). See also: O. Stier. *Electron ic and optical properties of quantum dots and wires* (Berlin Studies in Solid State Physics, Verlag Wissenshaft und Technik, Berlin 2001) and references cited therein
3. A.J. Williamson, A. Zunger. Phys. Rev. **B59**, 15819 (1999); **B61**, 1978 (2000)
4. A. Zunger. Phys. Stat. Solidi **A190**, 467 (2002) and references cited therein
5. S. Lee, L. Jönsson, J.W. Wilkins, G.W. Bryant, G. Klimeck, Phys. Rev. **B63**, 195318 (2001)
6. C. Cohen-Tannoudji, B. Diu, F. Laloe, *Quantum Mechanics* (John Wiley and Sons, New York 1977)
7. L.I. Schiff, *Quantum Mechanics* (Mc Graw-Hill, Singapore 1968)
8. D. Bohm, *Quantum Theory* (Prentice–Hall, Englewood Cliffs, NJ, USA 1951)
9. C. Beenacker and van Houten. Solid State Phys.**44**, 1 (1991) and references cited therein
10. J.D. Jackson, Classical Electrodynamics (John Wiley and Sons, New York 1975)
11. J.A. Brum, G. Bastard, Phys. Rev **B33**, 1420 (1986)
12. G. Bastard, Phys. Rev. **B30**, 3547 (1984)
13. J. Shah (ed.), *Hot Carriers in Semiconductor Nanostructures: Physics and Applications* (Academic Press, London, 1992)
14. P.Y. Yu, M. Cardona, *Fundamentals of Semiconductors: Physics and materials properties* (Springer-Verlag, Berlin, Second Edition, 1999)
15. B.K. Ridley, *Quantum Processes in Semiconductors* (Clarendon Press Oxford, 1988)
16. M. Babiker, B.K. Ridley, Superlatt. Microstruct. **2**, 287 (1986)
17. D. Morris, B. Deveaud, A. Regreny, P. Auvray, Phys. Rev. **B47**, 6819 (1993)
18. P. Sotirelis, K. Hess, Phys. Rev. **B49**, 7543 (1994)
19. M. Fricke, A. Lorke, J.P. Kotthaus, R. Madeiros-Ribeiro, P.M. Petroff, Europhys. Lett. **36**, 197 (1996)
20. Ph. Lelong, G. Bastard, Solid State Commun. **98**, 819 (1996)
21. D. P Phuong, PhD thesis, Paris 6 University (2005)
22. A. Vasanelli, PhD thesis, Paris 6 University (2002)
23. R. Buczko, F. Bassani, Phys. Rev. **B54**, 2667 (1996)
24. I. Magnusdottir, *Modeling of Phonon-and Coulomb-Mediated Capture Processes in Quantum Dots* (COM Technical University of Denmark, Lingby, Denmark, 2003)
25. I. Magnusdottir, A.V. Uskov, S. Bischoff, B. Tromborg, J. Mork, J. Appl. Phys. **92**, 5982 (2002)
26. R. Ferreira, G. Bastard, Appl. Phys. Lett. **74**, 2818 (1999)
27. K. Gündogdu, K.C. Hall, T.F. Boggess, G.D. Deppe, O.B. Shchekin, Appl. Phys. Lett. **85**, 4570 (2004)
28. S. Trumm, W. Besseli, H.J. Krenner, D. Schuh, M. Bichler, J.J. Finley, M. Betz, Appl. Phys. Lett. **87**, 153113 (2005)
29. O. Verzelen, S. Hameau, Y. Guldner, J.M. Gérard, R. Ferreira, G. Bastard, Jpn J. Appl. Phys. **40**, 1941 (2001)
30. S. Hameau, Y. Guldner, O. Verzelen, R. Ferreira, G, Bastard, J. Zeman, A. Lemaitre, J.M. Gérard, Phys. Rev. Lett. **83**, 4152 (1999)
31. I. Magnusdottir, A.V. Uskov, R. Ferreira, G. Bastard, J. Mork, B. Tromborg, Appl. Phys. Lett. **18**, 4318 (2002)
32. M. Glanemann, V.M. Axt, T. Kuhn, Phys. Rev. **B72**, 045354 (2005)
33. L. Chu, A. Zrenner, G. Böhm, G. Abstreiter, Appl. Phys. Lett. **75**, 3599 (1999)
34. N. Horiguchi, T. Futatsugi, Y. Nakata, N. Yokoyama, T. Mankad, P.M. Petroff, Jpn. J. Appl. Phys. Part I **38**, 2559 (1999)
35. H.C. Liu, M. Gao, J. McCaffrey, Z.R. Wasilewski, S. Faffard, Appl. Phys. Lett. **78**, 79 (2001)
36. S.F. Tang, S.Y. Lin, S.C. Lee, Appl. Phys. Lett. **78**, 2428 (2001)
37. L. Rebohle, F. Schrey, S. Hofer, G. Strasser, K. Unterrainer, Appl. Phys. Lett. **81**, 2079 (2002)
38. S. Maimon, E. Finkman, G. Bahir, S.E. Schacham, J.M. Garcia, P.M. Petroff, Appl. Phys. Lett. **73**, 2003 (1998)
39. S. Sauvage, P. Boucaud, T. Brunhes, V. Immer, E. Finkman, J.M. Gérard, Appl. Phys. Lett. **78**, 2327 (2001)
40. Z. Ye, J.C. Campbell, Z. Chen, E.T. Kim, A. Madhukar, J. Appl. Phys. **92**, 7462 (2002)
41. L. Chu, M. Arzberger, G. Böhm and G. Abstreiter, J. Appl. Phys. **85**, 2355 (1999)
42. J.S. Kim, P.W. Yu, J.Y. Leem, M. Jeon, S.K. Noh, J.I. Lee, G.H. Kim, S.K. Kang, J.S. Kim, S.G. Kim, J. Appl. Phys. **91**, 5055 (2002)
43. K.W. Berryman, S.A. Lyon, M. Segev, Appl. Phys. Lett. **70**, 1861 (1997)
44. M.V. Maximov, A.F. Tsatsul'nokov, B.V. Volovik, D.A. Bedarev, A.Y. Egorov, A.E. Zhukov, A.R. Kovsh, N.A. Bert, V.M. Ustinov, P.S. Kop'ev, Z.I. Alferov, N.N. Ledentsov, D. Bimberg, I.P. Soshnikov, P. Werner, Appl. Phys. Lett. **75**, 2347 (1999)

45. J. Phillips, K. Kamath, P. Bhattacharya, Appl. Phys. Lett. **72**, 2020 (1998)
46. B. Aslan, H.C. Liu, M. Korkusinski, S.J. Cheng, P. Hawrylak, Appl. Phys. Lett. **82**, 630 (2003)
47. E. Finkman, S. Maimon, V. Immer, G. Bahir, S.E. Schacham, F. Fossard, F.H. Julien, J. Brault, M. Gendry, Phys. Rev. **B63**, 045323 (2001)
48. E.T. Kim, A. Madhukar, Z. Ye, J.C. Campbell, Appl. Phys. Lett. **74**, 3277 (1999)
49. S.W. Lee, K. Hirakawa, Y. Shimada, Appl. Phys. Lett. **75**, 1428 (1999)
50. Ph. Lelong, S.W. Lee, K. Hirakawa, H. Sakaki. Physica **E7**, 174 (2000)
51. B.F. Levine, J. Appl. Phys. **74**, R1 (1993)
52. F.F. Schrey, L. Rebohle, T. Müller, G. Strasser, K. Unterrainer, D.P. N'guyen, N. Regnault, R. Ferreira, G. Bastard, Phys. Rev. **B72**, 155310 (2005)
53. D.P. N'guyen, N. Regnault, R. Ferreira, G. Bastard, Phys. Rev. **B71**, 245329 (2005)
54. (D. Bouwmeester, A. Ekert, A. Zeilinger (eds). *The Physics of Quantum Information* (Springer Verlag, Berlin 2000)
55. F. Rossi (ed.), *Semiconductor Macroatoms: Basic Physics and Quantum-device Applications* (Imperial College Press, London, 2005)
56. A.V. Uskov, J. MCInerney, F. Adler, H. Schweizer, Appl. Phys. Lett. **72**, 58 (1998)
57. I. Magnusdottir, A.V. Uskov, S. Bischoff, J. Mork, Phys. Rev. **B67**, 205326 (2003)
58. U. Bockelmann, T. Egeler, Phys. Rev. **B46**, 15574 (1992)
59. A.L. Efros, V.A. Kharchenko, M. Rosen, Solid State Commun. **B93**, 281 (1995)
60. U. Bockelmann, G. Bastard, Phys. Rev. **B42**, 8947 (1990)
61. Y. Toda, O. Mariwaki, M. Nishioka, Y. Arakawa, Phys. Rev. Lett. **82**, 4114 (1999)
62. H. Htoon, D. Kulik, O. Baklenov, A.L. Holmes, Jr., T. Takagahara, C.K. Shih, Phys. Rev. **B63**, 241303 (2001)
63. C. Kammerer, G. Cassabois, C. Voisin, C. Delalande, Ph. Roussignol, A. Lemaitre, J.M. Gérard, Phys. Rev. **B65**, 33313 (2001). See also C. Kammerer, PhD thesis, Paris 6 University (2002)
64. R. Oulton, J.J. Finley, A.I. Tartakowski, D.J. Mowbray, M.S. Skolnick, M. Hopkinson, A. Vasanelli, R. Ferreira, G. Bastard, Phys. Rev. **B68**, 235301 (2003)
65. E.W. Bogaart, J.E.M. Haverkort, T. Mano, T. van Lippen, R. Nötzel, J.H. Wolter. Phys. Rev. **B72**, 195301 (2005)
66. H. Benisty, C.M. Sottomayor-Torres, C. Weisbuch, Phys. Rev. **B44**, 10945 (1991)
67. A. Vasanelli, R. Ferreira, G. Bastard, Phys. Rev. Lett. **89**, 216804 (2002)
68. O. Verzelen, R. Ferreira, G. Bastard, Phys. Rev. Lett. **88**, 146803 (2002)
69. V.M. Fomin, V.N. Gladilin, J.T. Devreese, E.P. Pokatilov, S.N. Balaban, S.N. Klimin, Phys. Rev. **B57**, 2415 (1998)
70. L. Besombes, K. Kheng, L. Marsal, H. Mariette, Phys. Rev. **B63**, 155307 (2001)
71. A. Vagov, V.M. Axt, T. Kuhn, Phys. Rev. **B66**, 165312 (2002)
72. R. Wetzler, A. Wacker, E. Schöll, J. Appl. Phys. **95**, 7966 (2004)
73. T.R. Nielsen, P. Gartner, F. Jahnke, Phys. Rev. **B69**, 235314 (2004)
74. H.H. Nilsson, J.-Z. Zhang, I. Galbraith, Phys. Rev. **B72**, 205331 (2005)
75. D. Chaney, M. Roy and P. A. Maksym, in *Quantum Dots: Fundamentals, Applications, and Frontiers*, ed. by B. Joyce (Springer Verlag Berlin 2005)
76. F. Adler, M. Geiger, A. Bauknecht, F. Scholz, H. Schweizer, M.H. Pilkhun, B. Ohnesorge, A. Forchel, J. Appl. Phys. **80**, 4019 (1996)
77. B. Ohnesorge, M. Albrecht, J. Oshinowo, A. Forchel, Y. Arakawa, Phys. Rev. **B54**, 11532 (1996)
78. S. Grosse, J.H.H. Sandmann, G. von Plessen, J. Feldmann, H. Lipsanen, M. Sopanen, J. Tulkki, J. Ahopelto. Phys. Rev. **B55**, 4473 (1997)
79. S. Marcinkevicius, R. Leon, Phys. Rev. **B59**, 4630 (1999)
80. J.H.H. Sandmann, S. Grosse, G. von Plessen, J. Feldmann, G. Hayes, R. Phillips, H. Lipsanen, M. Sopanen, A. Aholpeto, Phys. Stat. Sol. **A164**, 421 (1997)
81. D. Morris, N. Perret, S. Faffard, Appl. Phys. Lett. **75**, 3593 (1999)
82. S. Raymond, K. Hinzer, S. Fafard, J.L. Merz, Phys. Rev. **B61**, 16331 (2000)
83. C. Delerue, M. Lannoo, *Nanostructures Theory and Modelling* (Nanoscience and Technology, Springer-Verlag, Berlin, 2004)
84. I.P. Marko, A.D. Andreev, A.R. Adams, R. Krebs, J.P. Reithmaier, A. Forchel, Elect. Lett. **39**, No. 1 (2003)
85. R.J. Warburton, B. Urbaszek, E.J. McGhee, C. Schulhauser, A. Hogele, K. Karrai, A.O. Govorov, J.M. Garcia, B.D. Gerardot, P.M. Petroff, Nature (London) **427**, 135 (2004)
86. B. Urbaszek, E.J. McGhee, M. Krüger, R.J. Warburton, K. Karrai, T. Amand, B.D. Gerardot, P.M. Petroff, J.M. Garcia, Phys. Rev. **B69**, 035304 (2004)
87. M.C. Bödefeld, R.J. Warburton, K. Karrai, J.P. Kotthaus, G. Madeiros-Ribeiro, P.M. Petrofff, Appl. Phys. Lett. **74**, 1839 (1999)
88. A. Wojs, P. Hawrilack, Phys. Rev. **B55**, 13066 (1997)
89. A.O. Govorov, R.J. Warburton, K. Karrai, Phys. Rev. **B67**, 241307 (2003)
90. R.W. Helmes, M. Sindel, L. Borda, J. Van Delft, Phys. Rev. **B72**, 125301 (2005)
91. J.M. Smith, P.A. Dalgarno, R.J. Warburton, A.O. Govorov, K. Karrai, B.D. Gerardot, P.M. Petroff, Phys. Rev. Lett. **94**, 197402 (2005)